

Machine Learning Parameterization of the Multi-scale Kain-Fritsch (MSKF) Convection Scheme and stable simulation coupled in WRF using WRF-ML v1.0

Xiaohui Zhong^{1,*}, Xing Yu², and Hao Li^{1,*}

¹Fudan University, Shanghai, 200433, China

²Shenzhen Institute of Artificial Intelligence and Robotics for Society, Guangdong, 518000, China

*These authors contributed equally to this work.

Correspondence: Xing Yu (yuxing@cuhk.edu.cn)

Abstract. Warm-sector heavy rainfall ~~often occurs along the coast of South China, and it is usually localized and long-lasting, making it challenging to predict.~~ High-resolution along the South China coast poses significant forecasting challenges due to its localized nature and prolonged duration. To improve the prediction of such high-impact weather events, high-resolution numerical weather prediction (NWP) models are increasingly used to better resolve topographic features and forecast such high-impact weather events more accurately represent topographic effects. However, ~~when the grid spacing becomes comparable to the length scales of convection, known as the gray zone, the turbulent eddies in~~ as these models' grid spacing approaches the scale of convective processes, they enter a "gray zone" where the models struggle to fully resolve the turbulent eddies within the atmospheric boundary layer ~~are only partially resolved and parameterized to some extent. Whether using a,~~ necessitating partial parameterization. The appropriateness of applying convection parameterization (CP) scheme in the schemes within this gray zone remains controversial. Scale-aware CP schemes are developed to enhance To address this, scale-aware CP schemes have been developed to improve the representation of convective transport ~~within the gray zone. The.~~ Among these, the multi-scale Kain-Fritsch (MSKF) scheme ~~includes modifications that allow for its effective implementation at a grid resolution enhances the traditional Kain-Fritsch (KF) scheme, incorporating modifications that facilitate its effective application at spatial resolutions~~ as high as 2 km. In recent years, there has been an increasing application of machine learning (ML) models ~~to~~ across various domains of atmospheric sciences, including ~~the replacement of efforts to replace conventional~~ physical parameterizations with ML models. This work ~~proposes~~ introduces a multi-output bidirectional long short-term memory (Bi-LSTM) model ~~as a intended to~~ replace the scale-aware MSKF CP scheme. The Data for training and testing the model are generated using the Weather Research and Forecast (WRF) model ~~is used to generate training and testing data~~ over South China at a horizontal resolution of 5 km. Furthermore, ~~the WRF model is~~ this work evaluates the performance of the WRF model coupled ~~with the ML-based CP scheme and compared with WRF simulations with original~~ ML-based CP scheme against simulations with traditional MSKF scheme. The results demonstrate that the Bi-LSTM model can achieve high accuracy, indicating the ~~potential use~~ promising potential of ML models to substitute the MSKF scheme in the gray zone.

1 Introduction

Warm-sector heavy rainfall often occurs ~~during the pre-flood seasons~~ in South China ~~due to the influence of~~ during the pre-flood
25 season, primarily influenced by the East Asian summer monsoon (Ding, 2004). These rainfall events are ~~localized and are~~
~~characterized by high precipitation intensity but limited spatial coverage. However, despite being small size, characterized by~~
intense and localized precipitation over limited area. Despite their small scale, such unexpected and extreme warm-sector rain-
fall can cause significant damage, ~~resulting in including~~ flooding homes and vehicles, destroying crop fields, and endangering
lives, ~~with costs amounting to millions or~~ leading to economic losses ranging from millions to even billions of dollars (Tao,
30 1981; Zhao et al., 2007; Zhong et al., 2015). Accurately predicting warm-sector heavy rainfall ~~using with~~ Numerical Weather
Prediction (NWP) models is challenging due to the complex interaction ~~between the influence of~~ of various factors, such as the
low-level jet (LLJ), land-sea contrast, topography, and urban landscape (Zhong and Chen, 2017; Luo et al., 2017; Jian et al.,
2002; Di et al., 2006; Xia and Zhao, 2009; Zhang and Ni, 2009). The ~~land surface in the~~ complex terrain and heterogeneous land
surface of South China region ~~is characterized by complex terrain and heterogeneity, which play a crucial role in promoting~~
35 ~~more active convections~~ are crucial in promoting active convection. Previous studies (Giorgi et al., 2016; Mishra et al., 2018;
Schumacher et al., 2020; Onishi et al., 2023) have ~~shown demonstrated~~ that higher spatial resolution improves the perfor-
mance of convective rainfall forecasts by ~~resolving topographic characteristics more accurately~~. Recognizing more accurately
resolving topographic features. Acknowledging the importance of resolution in forecasting severe convective weather, both the
Chinese government and the community have ~~shown increased support for developing~~ increasingly supported the development
40 of high-resolution operational forecast models specifically designed for warm-sector rainstorms and sudden local rainstorms.
In early 2017, the China Meteorological Administration (CMA) ~~initiated the development of a robust framework to evaluate~~
~~the forecast accuracy~~ launched an initiative to develop a comprehensive framework for evaluating the forecast performance
of all available models, including high-resolution regional models, and ~~to develop~~ advancing key technologies for forecasting
high-impact weather ~~forecasting~~.

45 ~~With the increased availability computational resources, there has been a growing trend of using~~ The increased computational
resources has facilitated a shift towards the implementation of regional NWP models with increasingly finer grid spacings, typ-
ically ~~ranging from within the range of~~ 1 to 10 km. However, when the model grid spacing ~~becomes comparable to the size~~
approaches the scale of convection, ~~which is known as the gray zone entering the so-called "gray zone"~~ (Wyngaard, 2004; Hong
and Dudhia, 2012), cumulus convection ~~that was previously unresolved becomes~~ transitions from being completely unresolved
50 to partially resolved. ~~In theory, unless~~ Theoretically, the accurate representation of the smallest turbulent scales, achievable
only through Direct Numerical Simulation (DNS) ~~is used to accurately capture the smallest turbulent scales with a resolution~~
~~of at resolutions from~~ millimeters to centimeters (Jeworrek et al., 2019), still requires the use of parameterization of turbulence
or convection ~~remains necessary for in~~ weather modeling. ~~Nevertheless, there is controversy about whether~~ There is ongoing
debate regarding the efficacy of employing convection parameterization (CP) ~~should be used in within~~ the gray zone. ~~Some~~
55 ~~previous studies (Chan et al., 2013; Johnson et al., 2013) reducing the~~ Several studies (Chan et al., 2013; Johnson et al., 2013)
have found that reducing horizontal grid spacing to below 4 km while using CP scheme ~~does not yield any improvement,~~

~~and in some cases even worsens~~, does not enhance and may even degrade, precipitation forecast performance. In contrast, Schwartz (2014) other studies (Lean et al., 2008; Roberts and Lean, 2008; Clark et al., 2012) showed that forecasts with a horizontal grid spacing of 1 km provide a, where convection is explicitly resolved, yielded more accurate spatial representation of accumulated rainfall over 48 hours compared to forecasts with using 12 km and 4 km grid spacing. ~~These conflicting findings typically arise when the CP scheme is applied at scales outside of its designed scales or when it is abruptly disabled at a resolution of approximately 3–5 km spacings.~~ This discrepancy in research findings, with some indicating no benefit from finer grid spacing and others suggesting improved forecast accuracy, seems to stem from the application of the CP at scales beyond its originally intended operational range. Therefore, it remains unclear if utilizing any CP schemes in the gray zone is effective for predicting localized warm-sector heavy rainfall.

To enhance ~~simulations prediction accuracy~~ in the gray zone, researchers ~~have~~ have developed scale-aware CP schemes. These schemes dynamically parameterize convective processes based on the horizontal grid spacing ~~and ensure a smooth transition across~~, thus facilitating seamless transitions between different spatial scales. A ~~study conducted by (Jeworrek et al., 2019)~~ pivotal study by Jeworrek et al. (2019) demonstrated that two specific scale-aware CP schemes, namely Grell-Freitas (Grell and Freitas, 2014) and multi-scale Kain-Fritsch (MSKF) (Zheng et al., 2016), outperform surpassed conventional CP schemes in terms of precipitation predicting both the timing and intensity of precipitation over the Southern Great Plains of the United States. ~~Despite the growing use~~ Additionally, Ou et al. (2020) showed that the MSKF scheme outperformed other CP schemes, including Grell-3D Ensemble (Grell and Dévényi, 2002) and New Simplified Arakawa-Schubert (Han and Pan, 2011), in precipitation simulation. This was evidenced by its lower root mean squared error (RMSE) values when compared against in-situ observations and satellite data. Despite the increasing adoption of these scale-aware schemes due to their superior performance, it is important to note that they also depend crucial to acknowledge that their efficacy also rely on various empirical parameters (Villalba-Pradas and Tapiador, 2022). Hence, the development of CP schemes specific to Therefore, developing specialized CP schemes for the gray zone in NWP models still presents significant challenges continues to be a significant challenge.

In recent years, ~~there has been a growing an increasing~~ number of studies ~~investigating have investigated~~ the use of machine learning (ML) models as ~~an alternative alternatives~~ to conventional physics-based CP schemes. These ML-based parameterization schemes have the potential to be effective at ~~schemes have demonstrated potential for efficacy across~~ various horizontal resolutions ~~because they are trained using data generated from models with~~, benefiting from being trained on data from simulations that operate at varying grid resolutions (Yuval and O’Gorman, 2020). Unlike conventional CP schemes, which often rely on assumptions like such as convective quasi-equilibrium (Arakawa, 2004), ML-based parameterization schemes do not ~~depend on require~~ such assumptions. ~~Random~~ Notably, random forests (RFs) and fully-connected (FC) neural networks (NNs) have ~~been the two most frequently employed become predominant~~ ML models for ~~convective parameterization (CP) schemes in prior research. RFs automatically impose CP schemes in previous studies. RFs offer the advantages of inherently enforcing physical constraints, including such as energy conservation and non-negative surface precipitation, which are crucial for essential for maintaining stable simulations. O’Gorman and Dwyer (2018) demonstrated that RFscan maintain stability and accurately reproduce essential climate statistics by training them to mimic the moist convection of RFs’ capability to emulate moist convection in~~ an aquaplanet general circulation model (GCM). ~~More recently, maintaining stability and effectively~~

reproducing key climate statistics. Furthermore, Yuval and O’Gorman (2020) employed the coarse-grained output ~~of from~~ a high-resolution three-dimensional (3D) GCM model, simulated on an idealized equatorial beta plane, to train the RF parameterization. They showed that the RF parameterization is capable of reproducing the climate of the high-resolution simulation ~~when used at coarse resolution~~ at coarser resolutions. However, FC NNs offer several advantages over RFs, such as the potential for higher accuracy and ~~reduced lower~~ memory requirements. ~~In their pioneering work, Krasnopolsky et al. (2013) formulated~~ Krasnopolsky et al. (2013) introduced a stochastic CP scheme using an ensemble of 3-layer NNs, ~~which were trained using~~ trained with data generated by a cloud-resolving model (CRM) ~~over a small area in the tropical Pacific Ocean during a four-month period of~~ during the TOGA-COARE ¹. ~~The results revealed that the NN-based parameterization yielded~~ reasonable and promising experiment, demonstrating its capacity for generating reasonable decadal climate simulations across a broader tropical Pacific region when incorporated into the National Center of Atmospheric Research (NCAR) Community Atmospheric Model (CAM). ~~Gentine et al. (2018) utilized~~ Similarly, Gentine et al. (2018) leveraged deep NN (DNN) trained on data from idealized and aquaplanet simulations performed using the SuperParameterized Community Atmosphere Model (SPCAM) ~~over an aquaplanet to train a deep NN (DNN).~~ The DNN predicts temperature and moisture tendencies ~~influenced~~ by due to convection and clouds, ~~along with as well as~~ the cloud liquid and ice water contents. Additionally, Rasp et al. (2018) successfully ~~incorporated~~ implemented an NN-based parameterization ~~into in~~ a global GCM on an aquaplanet. ~~They conducted, conducting~~ stable prognostic simulations for multiple years, accurately reproducing over multiple years that accurately reproduced the climatology of SPCAM and capturing crucial aspects of variability, including extreme precipitation and realistic tropical waves. However, Rasp (2020) also found that minor ~~modifications~~ changes to the configuration rapidly led to ~~unpredictable blow-ups in simulation.~~ Therefore, addressing the instability of NN parameterization in GCMs is necessary simulation instabilities, underscoring the need to address the robustness of NN parameterizations in GCMs. Yuval et al. (2021) developed a FC NN to that predicts ~~the~~ subgrid fluxes instead of tendencies, incorporating ~~the~~ physical constraints from coarse-grained high-resolution atmospheric simulation in an idealized domain. Brenowitz and Bretherton (2018, 2019) proposed a novel loss function ~~that minimizes the~~ designed to minimize accumulated prediction error over multiple time steps ~~instead of a single one.~~ They further ensured to enhance long-term stability and accuracy, by excluding upper atmospheric humidity and temperature from the ~~inputs.~~ However input. Nonetheless, the approach of removing ~~particular certain~~ variables from the ~~inputs input~~ is relatively rudimentary, demanding additional research to enhance the stability of NN-based parameterizations when integrated into the model.

~~In addition, previous studies have mainly~~ Previous studies have predominantly used FC NNs to emulate convection. ~~However,~~ there exist other, while more advanced NN structures ~~that~~ have the potential to achieve higher accuracy. In a ~~recent~~ pioneering study, Han et al. (2020) ~~made an initial attempt to employ~~ explored the use of a deep residual convolutional NN (ResNet) (He et al., 2016) for ~~emulating the emulation of~~ convection and cloud parameterization in the SPCAM model using a realistic configuration. They compared the performance of ResNet with ~~other various~~ various NN architectures, ~~such as including~~ a FC

¹TOGA-COARE is an acronym for Tropical Ocean Global Atmospheres/Coupled Ocean Atmosphere Response Experiment. It is an international research program that investigates the interaction or coupling of the ocean and atmosphere in the western Pacific warm pool region from November 1992 to February 1993, encompassing 120 days of field experiments involving the deployment of oceanographic ships, moorings, drifters, and Doppler radars (ship, land, air).

DNN, a DNN with skip connections, and a convolutional NN (CNN) without skip connections. The results ~~of their comparison~~
125 ~~demonstrated that both ResNet and CNN revealed that ResNet and CNNs~~ without skip connections outperformed ~~the FC NN~~
~~and the DNN FC NNs and DNNs~~ with skip connections in ~~terms of~~ accuracy, with ~~the performance of ResNet and CNN~~
~~ResNet and CNNs~~ without skip connections ~~exhibiting similar~~ showing comparable performance. This finding highlights the
~~crucial~~ significant role of convolutions in ~~achieving higher accuracy. Another study conducted by Yao et al. (2023) compared~~
~~various enhancing accuracy. Furthermore, Yao et al. (2023) evaluated multiple~~ ML model structures for ~~emulating simulating~~
130 atmospheric radiative transfer processes, ~~including encompassing~~ FC NNs, CNNs, bidirectional recurrent-based NNs (RNNs),
transformer-based NNs (Vaswani et al., 2017), and Fourier Neural Operators (FNO (Li et al., 2020)). Their results ~~revealed that~~
~~models with ability to perceive~~ indicated that models capable of perceiving global context of the entire atmospheric column
significantly outperformed FC NNs and CNNs. Particularly, the bidirectional long short-term memory (Bi-LSTM) achieved
the highest levels of accuracy. Similar to radiative transfer modeling, Han et al. (2020) also emphasized the importance of
135 ML having a global perspective of the entire atmospheric column for ML models in convection modeling. ~~Modifying They~~
~~demonstrated that increasing~~ the depths of CNNs from 4 to 22 layers ~~led to an increase in model accuracy. This improvement~~
~~is significantly improved model accuracy, a benefit~~ primarily attributed to the expansion of the receptive field in deeper CNN
layers. ~~Thus Therefore~~, ML models that integrate both global and local perception capabilities are better suited for developing
ML-based CP schemes.

140 ~~Furthermore, all previous studies have predominantly focused on using~~ Previous research have mostly focused on replacing
CP schemes in GCM models with ML models for climate forecasting. ~~Moreover, the choice~~ The complexity of CP schemes
~~significantly influences the uncertainty in precipitation forecasts within in~~ weather forecasting models. ~~The complexity of~~
~~the CP schemes also surpasses those applied in climate models (Arakawa, 2004). This study employs ML models to simulate~~
~~convective processes for weather forecasting. We generate our dataset by running surpasses that in GCMs (Arakawa, 2004).~~
145 Generally, CP schemes in GCMs, whether in explicit or implicit form, assume that both the horizontal grid size and the temporal
intervals for physics implementation are significantly larger and longer compared to the grid size and duration of individual
moist-convective elements. In contrast, CP schemes in high-resolution models must account for dependencies on both the
model's resolution and the time interval for implementing the physics (Arakawa, 2004). The ultimate goal is to develop ML
models, based on data from super-parameterization or cloud-resolving models, to replace conventional CP schemes in weather
150 forecasting models. This replacement seeks to reduce uncertainties and improve the efficacy of ML parameterizations. This
study represents an initial effort to employ a ML model as an alternative to conventional CP schemes in weather forecasting
models. For our dataset, we used the Weather and Research Forecasting (WRF) (Skamarock et al., 2021) model ~~with the that~~
covers the South China region, incorporating the scale-aware MSKF scheme employed as the CP scheme. ~~Developed as a means~~
~~to mitigate the precipitation overestimation associated with the original KF scheme, the MSKF scheme serves as~~ The MSKF
155 scheme, an improved version of the Kain-Fritsch (KF) scheme (Kain and Fritsch, 1990, 1993; Kain, 2004). ~~The KF scheme~~
~~often initiates convection prematurely, which leads to an overprediction of precipitation, aims to mitigate the overestimation~~
of precipitation, address the premature convection trigger issue, particularly evident in overestimating precipitation
during summer. To address these issues, the MSKF incorporates a scale-dependent capability, such as modifying the formulation of

the convective adjustment timescale. This vital parameter ~~defines~~, which determines the intensity and duration of convection, ~~and the MSKF scheme made it dynamic and grid-resolution dependent (Zhang et al., 2021). The WRF model covers the South China region.~~ has been made dynamic and dependent on grid resolution (Zhang et al., 2021). Furthermore, we utilize a Bi-LSTM model to emulate the convective processes and couple it with the WRF model using-through the WRF-ML coupler developed by Zhong et al. (2023a). The performance of the ML-based CP scheme is evaluated in both offline and online settings.

165 The paper is structured as follows. Section 2 provides a description of the WRF model for data generation, as well as the input and output data of the ML model. In Section 3, the original and the ML-based MSKF scheme is introduced. The results for both offline and online testing of the ML-based MSKF scheme are presented in Section 4. Finally, Section 5 presents the summary and conclusion.

2 Data

170 2.1 Data generation

The dataset was generated by running the WRF model version 4.3 (Skamarock et al., 2019, 2021). The following subsections provide a comprehensive explanation of the WRF model configurations, as well as the input and output variables employed in the development of the ML-based CP scheme.

The WRF model is compiled using the GNU Fortran (gfortran version 7.5.0) compiler with the "dmpar" option. The WRF model is run using the domain configuration illustrated in Figure 1. The WRF model is configured with a single domain consisting of 44000 grid points, with a horizontal grid spacing of 5 km and dimensions of 220×200 grid points in the west-east and north-south directions. The model consists of 45 vertical levels (i.e., 44 vertical layers), with a model top at 50 hPa. Additionally, the WRF model is configured with physics schemes, including WSM 6-class graupel scheme (Hong and Lim, 2006) for microphysics, Bougeault-Lacarrère (BouLac) scheme (Bougeault and Lacarrère, 1989) for planetary boundary layer (PBL) mixing, the Monin-Obukhov (Janjic) surface layer scheme (Janjic, 1996), the Unified Noah model (Livneh et al., 2011) for land surface, RRTMG for both shortwave and longwave radiation (Iacono et al., 2008), and MSKF (Zheng et al., 2016) for cumulus. The time step used for all WRF simulations is set to 15 seconds.

The initial and boundary conditions for this work were derived from the ERA5 reanalysis dataset, which was provided by the European Centre for Medium-range Weather Forecast (ECMWF) (Hersbach et al., 2020). The ERA5 reanalysis dataset used in this study has a horizontal resolution of 0.25° and consists of 29 pressure levels below 50 hPa. To create a dataset for developing the ML model, the WRF simulations were initialized at 12 UTC and conducted 9 times every 2 days, specifically from May 20th, 2022 to June 5th, 2022. Throughout the simulations, the MSKF scheme was called every 5 model minutes, generating outputs at each call. The simulations ran for 36 hours each time, with the first 24 hours used for training and the

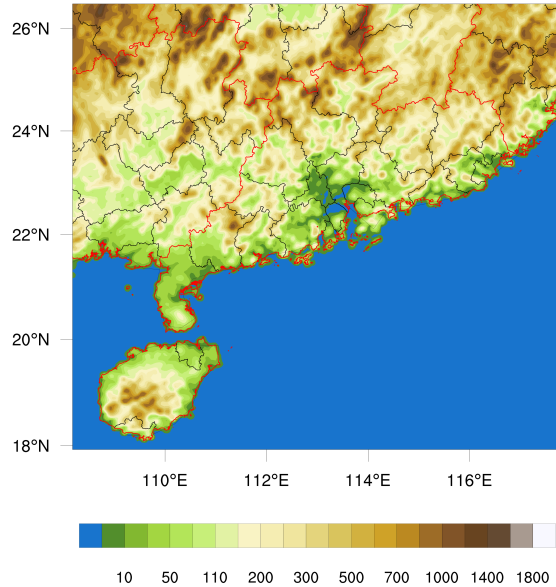


Figure 1. Digital elevation data of the single WRF domain with horizontal resolution at $5 \times 5^\circ$. Red lines are the province borderlines, and black lines are the city borderlines.

last 12 hours for validation. Therefore, the total number of training samples is $114,444,000^2$ while the offline validation set
 190 contains $57,024,000^3$ samples.

Furthermore, ~~considering that the offline performance might not necessarily reflect its performance in online setting~~ given the possible discrepancy between offline performance, we conducted experiments ~~by coupling that coupled~~ the ML-based MSKF scheme with WRF model ~~and comparing the results to the original WRF simulations to evaluate the online performance~~. This coupling aims at evaluating the online efficacy of the ML-based MSKF scheme. ~~The simulations were conducted by comparing it with the original WRF simulations. These simulations were performed~~ 4 times every 2 days, each lasting 36 hours with each simulation extending over a period of 168 hours (7 days). The initialization days spanned from June 12th, 2022 to June 18th, 2022.
 195

2.2 Input and output data

Table 1 presents a comprehensive list of the input and output variables used in this study, consistent with those utilized in the original MSKF scheme. There are ~~13~~ 17 variables exclusively used as input, while 9 variables serve as both input and output. ~~The output~~ Specifically, the output variable "raincv", representing the time-step precipitation due to convection ("raincv"), is calculated through multiplying the precipitation rate by the model's time step. ~~Out of~~ Among all the variables, 5 are two-

² $114,444,000 = 44000 \times 9 \times (24 \times 60 / 5 + 1)$

³ $57,024,000 = 44000 \times 9 \times 12 \times 60 / 5$

dimensional (2D) surface variables, while the remaining ones are 3D variables characterized by 44-layer vertical profiles. ~~Additionally~~ Moreover, the ML model used in this study incorporates 4 derived variables as input. These variables consist of a 2D Boolean variable indicating convection triggering based on ~~the values of "nca"~~, ~~pressure difference between each values, the pressure difference across~~ adjacent vertical levels, ~~the~~ saturated water vapor mixing ratio, and relative humidity. Furthermore, the output "w0avg", which depends on vertical wind component (w) and input "w0avg", is also included as an input to model. In total, the ML model utilizes 27 input variables.

The variable "nca" represents the cloud relaxation time and must be an integer multiple of the model time step. For all WRF model simulations conducted in this study, a fixed time step of 15 seconds is used. Thus, "nca" is expected to be ~~evenly~~ exactly divisible by 15. To eliminate dependence on the specific model time step, "nca" is divided by the model time step before normalization is applied during model training. Moreover, within the MSKF scheme, "nca" plays a crucial role in determining the triggering of convection. Convection is triggered when "nca" is ~~greater than or equal to~~ equal to or exceeds half of the model time step.

To ensure consistency with the dimensions of the 3D variables, the surface variables are padded by duplicating the values of the surface layer for all layers before feeding them into the model. Prior to utilizing the variables in the Bi-LSTM model for training and validation, normalization is applied to ensure uniformity in the magnitudes of all the variables. Each variable is divided by the maximum absolute value in the atmospheric column (for 3D variables) or at the surface (for surface variables).

Table 1. Definition of all the input and output variables, and whether they are surface or 3D variables and their corresponding units. There are 44 model layers.

| Type | Variable name | Definition | type | Unit |
|----------------------|-------------------------|-------------------------------------------------------------------------------------------------------|----------------|-------------------|
| Input | u | meridional wind component | 3D | m/s |
| | v | zonal wind component | 3D | m/s |
| | w | vertical wind component | 3D | m/s |
| | t | temperature | 3D | K |
| | qv | Water-water vapor mixing ratio | 3D | kg/kg |
| | p | pressure | 3D | Pa |
| | th | potential temperature | 3D | K |
| | dz8w | layer thickness | 3D | m |
| | rho | air density | 3D | kg/m ³ |
| | pi | Exner function, which is dimensionless pressure and can be defined as: $(\frac{p}{p_0})^{R_d/c_p}$ | | |
| | hfx | upward heat flux at surface | surface | W/m ² |
| | ust | u* in similarity theory | surface | W/m ² |
| | pblh | planetary boundary layer height | surface | m |
| <u>Derived Input</u> | <u>Pdiff</u> | <u>pressure difference between adjacent levels</u> | <u>3D</u> | <u>Pa</u> |
| | <u>qv_{sat}</u> | <u>saturated water vapor mixing ratio</u> | <u>3D</u> | <u>kg/kg</u> |
| | <u>rh</u> | <u>relative humidity</u> | <u>3D</u> | - |
| | <u>trigger</u> | <u>boolean trigger indicating convection triggering</u> | <u>surface</u> | - |
| Input and Output | rthcuten | potential temperature tendency due to cumulus parameterization | 3D | K/s |
| | rqvcuten | water vapor mixing ratio tendency due to cumulus parameterization | 3D | kg/kg/s |
| | rqqcuten | cloud water mixing ratio tendency due to cumulus parameterization | 3D | kg/kg/s |
| | rqruten | rain water mixing ratio tendency due to cumulus parameterization | 3D | kg/kg/s |
| | rqiuten | cloud ice mixing ratio tendency due to cumulus parameterization | 3D | kg/kg/s |
| | rqsuten | snow mixing ratio tendency due to cumulus parameterization | 3D | kg/kg/s |
| | w0avg | average vertical velocity | 3D | m/s |
| | nca | counter of the cloud relaxation time | 3D | s |
| | pratec | precipitation rate due to cumulus parameterization | surface | mm/s |
| Output | raincv | precipitation due to cumulus parameterization | surface | mm |

3 Method

220 This section describes the flow chart of original MSKF scheme for determining convection trigger, ML model structures and training, and the evaluation methods.

3.1 Description of original MSKF module

The MSKF scheme is a scale-aware adaptation of the KF CP scheme, ~~which was originally initially~~ developed by Kain and Fritsch (1990, 1993) and ~~later modified further refined~~ by Kain (2004). ~~The flow chart illustrating Figure 2 illustrates~~ the convection trigger process ~~in the original MSKF scheme is illustrated in Figure 2 within the MSKF scheme~~. At the beginning of each ~~call, the simulation step, the scheme evaluates the~~ variable "nca" ~~is examined to determine if exceeds or equals a threshold equal to half of the model~~ to ascertain whether it equals or surpasses a threshold, defined as half the model's time step (dt). ~~If Should "nca" is greater than or equal to equal or exceed the~~ half of dt, ~~the convective tendencies and precipitation rate do not require updating since convection is still active. If there is no need to update convective tendencies or precipitation~~ rates due to ongoing convection. In contrast, a "nca" ~~is smaller than the specified threshold, a 1-D cloud model within value below this threshold triggers~~ the MSKF scheme ~~is used to calculate various to employ a one-dimensional cloud model. This model calculates a set of~~ variables related to cloud ~~properties in order to determine whether convective should be triggered. These characteristics to evaluate the potential of convection triggering. Essential~~ variables include the lifting condensation level (LCL), convective available potential energy (CAPE), cloud top and base heights, and entrainment rates. ~~If convection is activated for a particular grid point, the MSKF scheme computes the convective tendencies and precipitation rate. On the other hand, if convection is not~~The LCL is crucial for determining the emergence of potential convective activities, with a lower LCL favoring more intense convection. CAPE quantifies the buoyant energy available to an air parcel for the formation of deep convective clouds upon reaching its Level of Free Convection (LFC) above the LCL, with higher CAPE values signifying a greater potential for intense convection. The cloud base is generally at the LCL, whereas the cloud top is defined at the altitude where buoyancy becomes negligible. Meanwhile, the vertical extent between the cloud base and top affect the cloud's growth and precipitation potential. The MSKF scheme requires surpassing a specific CAPE threshold to trigger convection. Furthermore, it assesses entrainment rates to measure the impact of ambient air on the evolution of convective system. At grid points where convection is triggered, the ~~MSKF scheme calculates both~~ convective tendencies and precipitation ~~rate remain at 0- rates; otherwise these values are set to zero.~~ However, the variable "w0avg" is ~~always updated regardless whether convection is triggered or not. As long as the convection remains active, consistently updated, regardless of convection status. Active convection leads to a decrement in~~ "nca" ~~is decremented~~ by one model time step ~~at each WRF model's time step~~ for each iteration within WRF model cycle.

3.2 Description of ML-based MSKF scheme

In the original MSKF scheme, ~~the atmospheric column is~~ atmospheric columns are processed sequentially, one at a time, until all horizontal grid points within the domain have been processed. In contrast, the ML-based MSKF scheme ~~performs~~

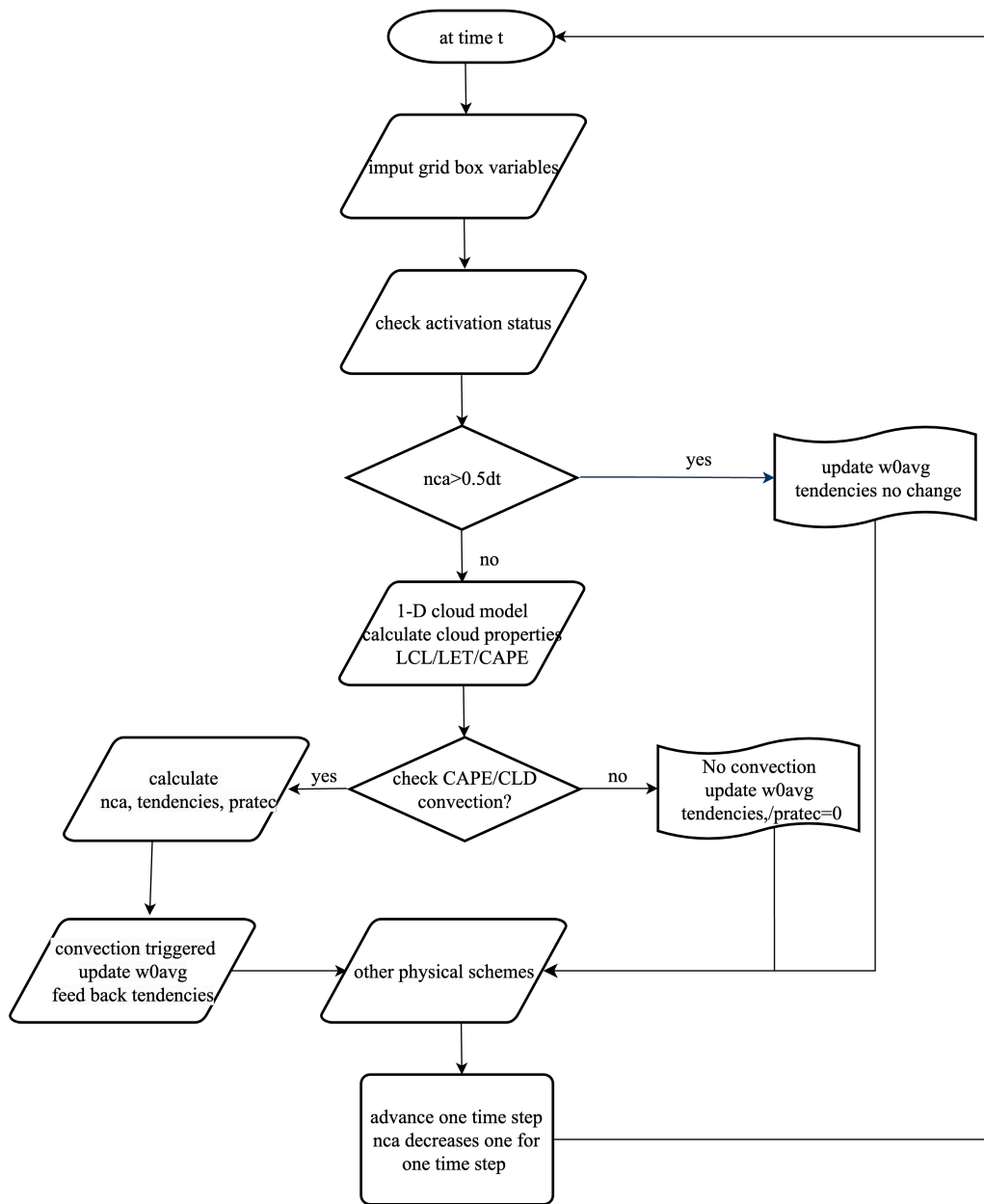


Figure 2. A flow chart outlining convection trigger process in the original MSKF scheme.

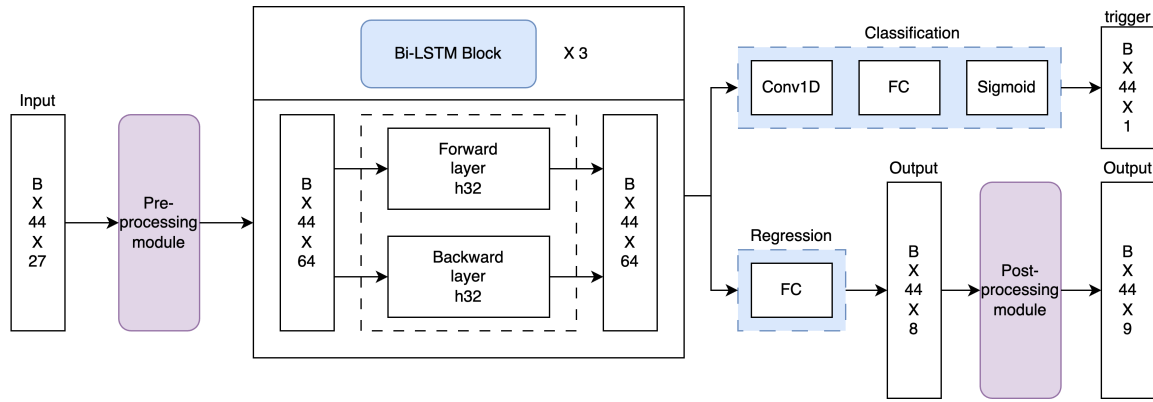


Figure 3. The architecture of the multi-output Bi-LSTM model for combined classification and regression predictions.

calculations on a batch (see Figure 3) of data processes data in batches, as indicated by "B" in Figure 3, consisting of 44 features and 27 features across 44 vertical layers. As a result, the input data has dimensions of $B \times 27 \times 44$. Before being fed into the ML model, the input data data undergoes pre-processing through a module incorporating a 1-dimensional (1D) convolutional layer. This module increases expands the feature dimension from 27 to 64. The subsequent following sections provide a comprehensive description of the structures of the ML model.

3.2.1 ML model structure

Predicting whether convection is triggered as well as modeling convective tendencies and precipitation rate precipitation rates are two main tasks in conventional CP schemes. Regression-based models alone may result in inconsistent tendencies, leading to conflicting signals for triggering convection at specific grid points. Similarly, models solely dependent on classification lack the capability to generate essential tendencies for an effective CP scheme. Therefore, the development of a ML-based CP scheme requires necessitates the integration of both a binary classification model for predicting the prediction of convection trigger and a regression model for modeling convective tendencies. Accordingly To address this, we propose a multi-output Bi-LSTM model that can simultaneously perform capable of concurrently conducting regression and classification predictions (Figure 3). Our proposed model consists of a shared Bi-LSTM layer for learning features, a classification subnetwork, and a regression subnetwork. The shared Bi-LSTM layer includes three repeated Bi-LSTM blocks, with each block containing a forward and a backward layer that have a feature dimension of 32. The classification subnetwork is composed of a 1×1 1D convolutional layer, a FC layer, and a Sigmoid activation layer. The output of the Sigmoid layer represents the probability distribution of the convection trigger. The binary cross-entropy loss function is employed as the cost function for this classification task. Meanwhile, the regression subnetwork incorporates a FC layer to output precipitation rate, "nca", and convective tendencies. Finally, the output of both subnetworks passes outputs from both subnetworks are the processed through a post-processing module to ensure physical consistency. The post-processing module is introduced in more detail in the following their physical consistency, with further details provided in the subsequent subsection.

3.2.2 Post-processing module

The post-processing module is designed to ensure physical consistency of all variables. ~~The~~ To achieve this, the following rules are applied: 1) ~~For~~ At grid points where the input "nca" is ~~greater than or equal to half~~ equal to or greater than half the value of dt, all other variables remain unchanged as they are still within the convection lifetime. 2) The output "nca" must be an integer. 3) ~~For~~ At grid points where convection is predicted to be inactive, all ~~other~~ corresponding output variables are ~~set~~ default to zero. In addition, the calculation of time-step convective precipitation (raincv) ~~is calculated as described~~ follows the methodology outlined in the previous section 2.2.

3.2.3 Model training

As our model incorporates both classification and regression tasks, we optimize its performance by minimizing a multi-task loss function (Ren et al., 2016). The loss function is defined as the sum of the binary cross entropy loss for the convection trigger and a weighted combination of the $L1$ loss for all output variables from the regression subnetwork. The specific formulation of the loss function is as follows:

$$L = \frac{1}{N_{cls}} \sum_{i,j} L_{cls}(p_{i,j}, p_{i,j}^{gt}) + \sum_c \lambda_c \frac{1}{N_{reg}} \sum_{i,j} p_{i,j}^{gt} L1_c \quad (1)$$

Here, i and j denote the grid points in the domain. $p_{i,j}$ represents the probability of convection being triggered. The ground-truth label $p_{i,j}^{gt}$ takes a value of 1 if convection is triggered and 0 otherwise. The classification loss L_{cls} is calculated using the binary cross entropy loss. For the regression loss of different variables c , λ_c functions as a weight that balances the output variables by considering their respective magnitudes. The term $p_{i,j}^{gt} L1_c$ indicates that the $L1$ regression loss is activated only for triggered grid points ($p_{i,j}^{gt} = 1$) and is disabled otherwise ($p_{i,j}^{gt} = 0$). Both loss terms are normalized by N_{cls} and N_{reg} , which correspond to the total number of grid points and the number of triggered grid points, respectively.

Adam optimizer (Kingma and Ba, 2014) is used with an initial learning rate of 0.003 update the parameters of the model. Furthermore, the plateau scheduler is implemented to decrease the learning rate by a factor of 0.5 when the loss fails to decrease for five epochs. The model is trained for 150 epochs using a batch size of 44000.

3.3 Evaluation methods

The ML-based MSKF scheme is evaluated in both offline and online settings. The offline performance of the ML-based MSKF scheme is evaluated by comparing it against the outputs of the original MSKF scheme using validation dataset, including rthcuten, rqvcuten, rqccuten, rqruten, nca, and pratec. The overall model performance metrics include ~~root-mean-squared error (RMSE)~~ RMSE and correlation coefficient. The mean absolute error (MAE) and mean bias error (MBE) per vertical layer were were calculated using the equation below:

$$MAE_l = \frac{1}{N} \sum_{i=1}^N |Y_{ML}(i, l) - Y(i, l)| \quad (2)$$

$$MBE_l = \frac{1}{N} \sum_{i=1}^N Y_{ML}(i, l) - Y(i, l) \quad (3)$$

where $Y(i, l)$ and $Y_{ML}(i, l)$ represent the outputs from the original MSKF scheme and ML-based MSKF scheme, respectively. Here, i denotes the horizontal grid point of a vertical profile, N is the number of the horizontal grid points in the domain, l represents the vertical layer index.

4 Results

4.1 Offline validation of the ML-based MSKF scheme

The offline validation was conducted using data that was not used during the training process. Figure 4 compares the cloud relaxation time (nca), precipitation rate (pratec), and convective tendencies predicted by both the original MSKF scheme and the ML-based MSKF scheme, respectively. To facilitate the comparison, the units of precipitation rate and temperature tendencies were multiplied by a factor of 86,400 (24 × 3600) to convert from converted to mm·sd⁻¹ and K·sd⁻¹ to from mm·ds⁻¹ and K·ds⁻¹, respectively, by applying a conversion factor of 86,400 (24 × 3600). Similarly, the water vapor mixing ratio (rqvcuten), cloud water mixing ratio (rqccuten), and rain water mixing ratio (rqrcuten) resulting from due to convection were multiplied by 86,400,000 (24 × 3600 × 1000) to convert from kg·kg⁻¹·s⁻¹ to g·kg⁻¹·d⁻¹. Among the output variables listed in Table 1, the variable w0avg is excluded as it is calculated using an equation with the ground truth as input in this offline validation. Hence, evaluating w0avg in the offline evaluation is unnecessary.

Among all the variables illustrated in Figure 4, the variable "nca" exhibits a significantly higher RMSE of 4.32, and its data points appear scattered with data points widely dispersed across a wide range of values. This suggests that accurately predicting convection poses a considerable challenge. Prior to plotting and performing statistical calculations To eliminate the dependency on time steps, "nca" is divided by the model's time step of 15 to eliminate the time step dependence seconds before proceeding with plotting and statistical evaluations. The precipitation rate demonstrates the highest correlation coefficient and the smallest spread minimal variability, as most data points cluster closely around the 1:1 line. In the case of While temperature and the four moisture tendencies , the data also displays some dispersion, but a majority of the data points remain close exhibit some degree of variability, the majority of data points align closely to the 1:1 line. The correlation coefficient of convection trigger is 0.91, not shown in Figure 4. Overall, the ML-based MSKF scheme shows a strong correlation with the original MSKF scheme for all the examined variables, with correlation coefficients consistently higher than 0.91. This indicates that the the ML-based MSKF scheme has the potential to replace the original scheme.

To gain obtain a comprehensive understanding of the vertical distribution of errors, Figure 5 illustrates presents the vertical profiles of statistics in error statistics associated with convective tendencies. The solid and dotted lines in the figure represent the MAE and MBE of tendencies at each vertical layer, respectively. Additionally, the shaded area corresponds to the 5th and 95th percentiles of differences between tendencies predicted by the ML-based MSKF predicted scheme and the original

MSKF scheme, respectively. The ~~vertical error distribution~~ distribution of vertical errors in all tendencies ~~is quite similar~~ exhibits a notable uniformity, with higher variance observed ~~among~~ within the pressure layers between 800 and 1,000 hPa. These pressure layers ~~corresponds~~ correspond to the atmospheric layer where convection occurs most frequently. Due to the
335 significantly lower cloud and rain content compared to water vapor in the atmosphere, the error magnitudes for rqcuten and rqruten are considerably ~~smaller than those~~ lower than those observed for rqcuten.

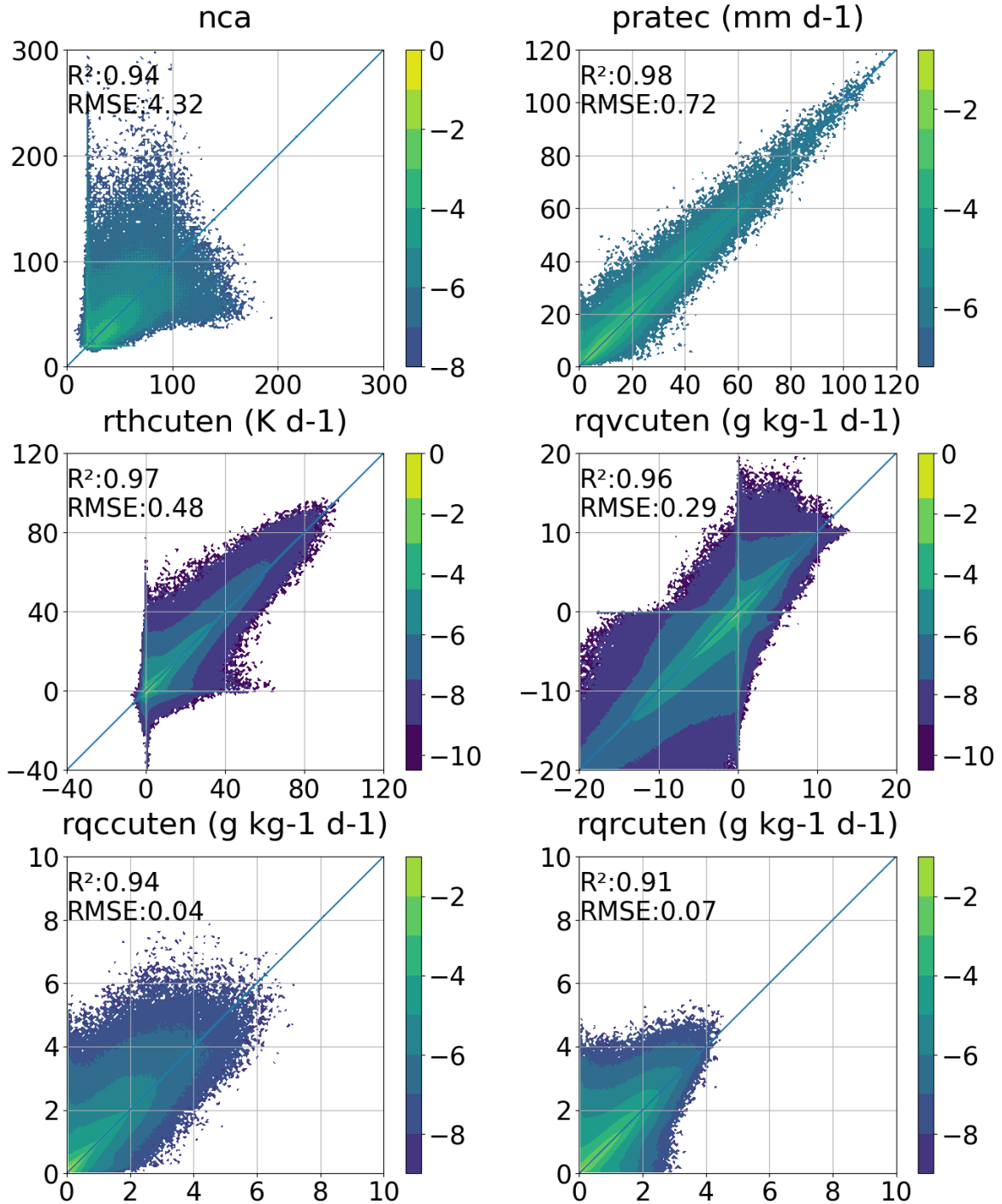


Figure 4. Comparison of the predicted (y axis) and true (x axis) nca, pratec, rthcuten (first column), rqvcuten (second column), rqccuten (third column), and rqrcuten for using validation data in the offline setting. [Colors indicate the proportion of samples across the entire testing dataset, with values on the colorbar normalized through the application of a logarithm base 10.](#)

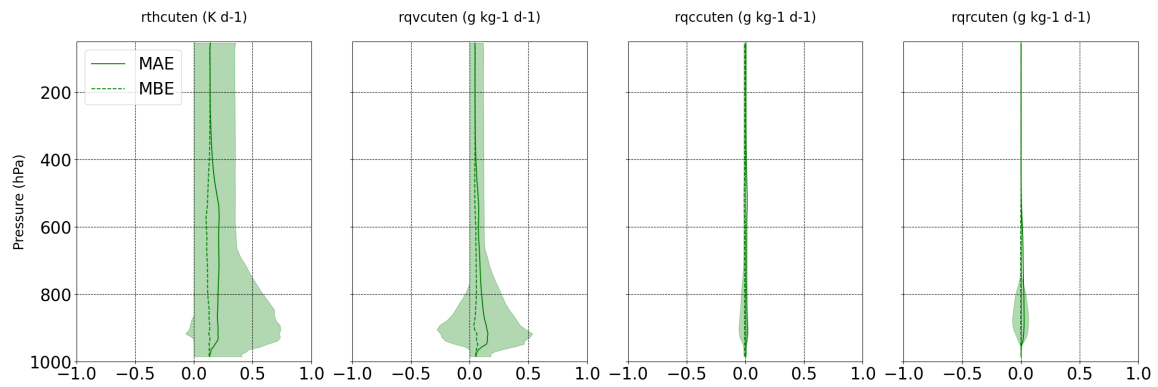


Figure 5. Vertical profiles of the statistics in rthcuten (first column), rqvcuten (second column), rqccuten (third column), and rqrcuten (fourth column) using validation data in the offline setting data using ML-based emulators. The solid and dotted lines show the MAE and MBE profile, respectively, and the shaded area indicates the 5th and 95th percentile of differences (prediction—target) at each layer.

4.2 Prognostic validation

This subsection presents the performance of the ML-based MSKF scheme in the online setting.

The ML-based MSKF scheme was integrated ~~as a replacement into the WRF model as a substitute~~ for the original MSKF scheme ~~in the WRF model to model convective effects. The to simulate convective processes. Utilizing the~~ WRF-ML coupler (Zhong et al., 2023a) ~~was used to incorporate the~~, this novel ML-based MSKF scheme ~~was seamlessly incorporated~~ into the WRF ~~model. Both~~ framework. A comparative analysis was conducted by initializing both the modified WRF model, ~~incorporating which incorporates~~ the ML-based scheme, and the original WRF model ~~were initialized~~ on June 12, 14, 16, and 18, 2022, ~~and run for 36 for simulations extending over 168~~ hours. It is worth mentioning that ~~this runtime was completely~~ independent ~~these simulations were performed independently~~ of the training dataset, ~~ensuring the evaluation of the scheme's~~ generalization capability.

~~In Figure 6 , Figure 6 presents~~ the averaged spatial forecasts ~~of the 4-day prediction from the for predictions generated~~ by the original WRF model ~~are presented. These results include accumulation of convective~~. These forecast results include ~~the accumulations of both convective precipitation (RAIN_C) and non-convective precipitation (RAIN_NC) over a 12-hour~~ period, ~~as well as along with~~ the 2-meter temperature ~~at 12, (T2M) at 24, and 36-72, 120, and 168~~ hours. The figure also ~~illustrate demonstrates~~ the mean absolute difference (MAD) between ~~the~~ WRF simulations coupled with the ML-based MSKF scheme and those ~~using utilizing~~ the original MSKF scheme. ~~The Within the spatial forecasts, red and blue patterns in the spatial forecasts represent the signify the~~ magnitudes of the forecast values. ~~In the spatial difference, red and blue patterns reveal forecasted values, whereas in the spatial differences, these colors denote~~ the positive and negative biases ~~of in~~ the ML-based simulations, respectively. ~~while green patterns suggest little to no difference compared to~~ Green patterns suggest ~~minimal deviation from~~ the original WRF simulations. ~~Additionally, Furthermore, we calculate~~ a domain-averaged MAD ~~is calculated~~ to evaluate the overall performance of the ML-based scheme in prognostic simulations. Generally, the ~~difference is small suggesting that the differences are small, indicating good agreement between~~ WRF simulations coupled with ~~the~~ ML-based MSKF scheme ~~agree well with the origiant and the original~~ WRF simulations. ~~Also, the difference does not increase as~~ the simulation time progresses, ~~as there is~~ Notably, the differences do not increase with the progression of simulation time, ~~as evidenced by~~ a comparable domain-averaged MAD at ~~36-168~~ forecast hours compared to that at ~~12-24~~ forecast hours. These findings ~~indicate suggest~~ that the ML-based MSKF scheme achieves stable prognostic simulations.

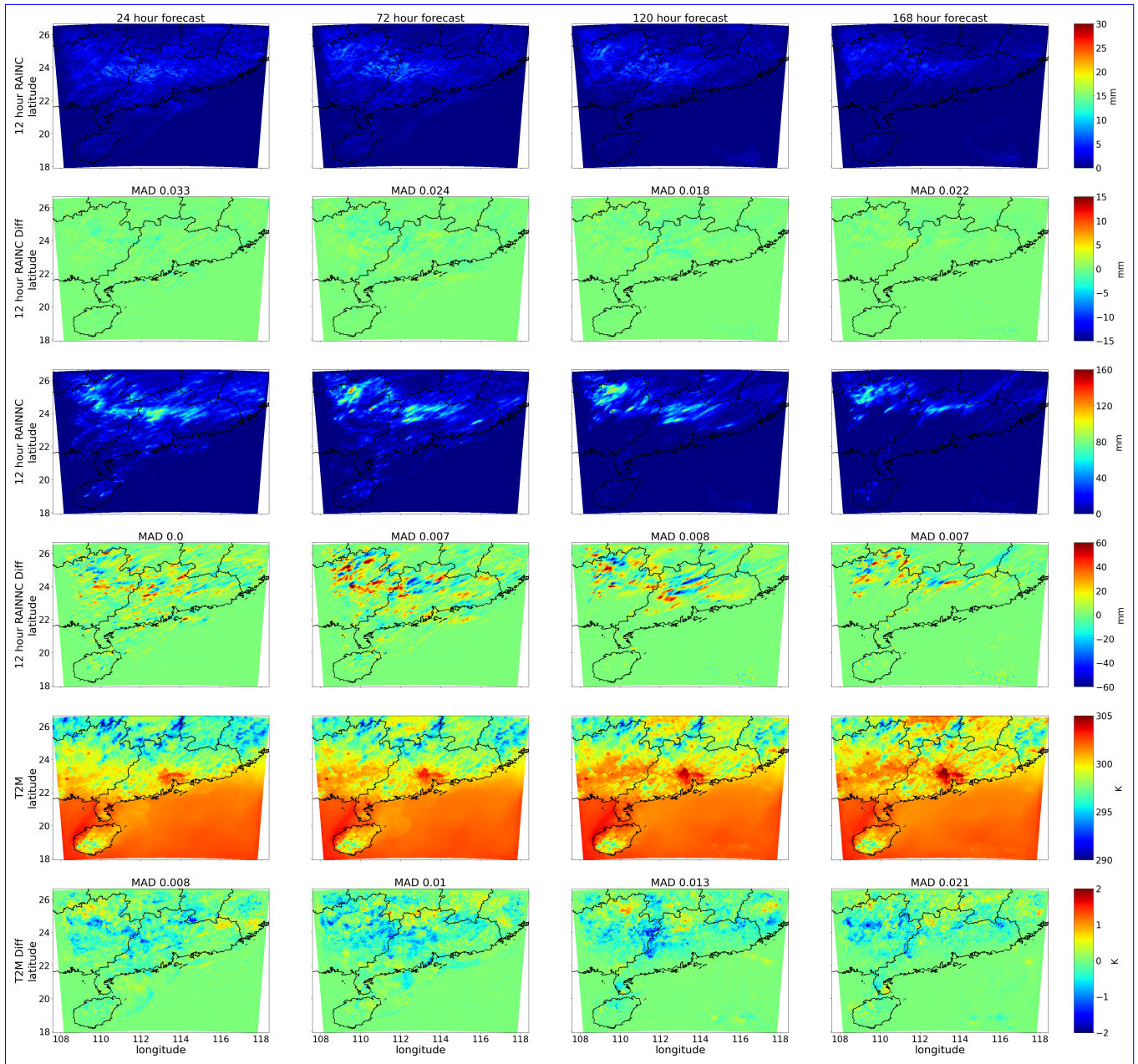


Figure 6. Spatial map of the average WRF simulations using the original MSKF scheme (in the first, third, and fifth rows) along with the average MAD between WRF simulations coupled with the ML-based MSKF scheme and WRF simulation with the original MSKF scheme (in the second, fourth and sixth rows). The simulations are shown for the 12-hour accumulated convective precipitation (*RAINNC*) in the first and second rows, the 12-hour accumulated non-convective precipitation (*RAINNC*) in the third and fourth rows, and the 2-meter temperature (*T2M*) at forecast lead times of 12-24 hours (first column), 24-72 hours (second column), and 36-120 hours (third column), and 168 hours (fourth column).

365 Figure 7 provides a comparative analysis of domain-averaged time series forecasts from both the original WRF simulations and WRF simulations coupled with the ML-based MSKF scheme. This comparison includes 6-hour accumulations of *RAINNC* and *RAINNC*, as well as *T2M* forecasts. The results demonstrate that WRF simulations coupled with the ML-based MSKF schemes are in close alignment with the original WRF simulations, particularly in capturing the diurnal variations of *RAINNC*, *RAINNC*, and *T2M*. Notably, the *T2M* forecasts demonstrate remarkable consistency, underscoring the efficacy of the ML-based MSKF scheme in maintaining the predictive accuracy of the original scheme.

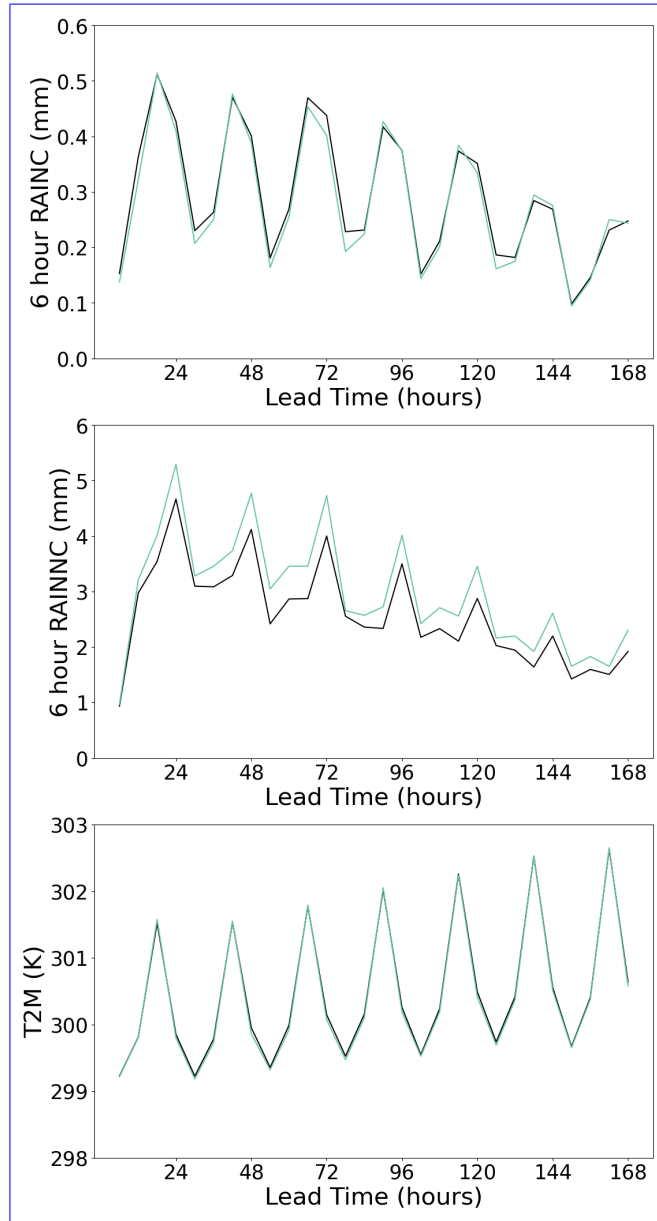


Figure 7. Comparison of domain-averaged forecasts derived from the original WRF simulations (black lines) and WRF simulations coupled with the ML-based MSKF scheme (light green lines) of 6-hour accumulated *RAINNC* (first row) and *RAINNC* (second row), along with *T2M* (third row).

5 Conclusions

370 In this paper, we proposed a multi-output Bi-LSTM model to ~~developing~~ develop a ML-based MSKF scheme for predicting convection trigger and reproducing the convective process in the gray zone. The model is trained ~~using data generated from on~~ data generated by the WRF simulations at a spatial resolution of 5 km, covering the South China region. The output variables of the ML-based MSKF scheme are identical to those of the original MSKF scheme, ~~which include encompassing~~ cloud relaxation time ("nca"), precipitation rate ("pratec"), time-step convective precipitation ("raincv"), and convective tendencies.

375 ~~In the~~ This ML-based scheme ~~, the ensures~~ physical consistency among all output variables ~~is considered and encoded as by~~ incorporating a post-processing module to refine the output from the Bi-LSTM model. Offline validation demonstrates the excellent performance of the ML-based MSKF scheme. Furthermore, the ML-based MSKF scheme is coupled with the WRF model using WRF-ML coupler. The WRF simulations coupled with the ML-based MSKF scheme is compared against the WRF simulation with the original MSKF scheme. Results shows that the ML-based scheme can generate forecasts similar to

380 the original ML scheme in online settings, showing the potential substitution of the MSKF scheme by ML models in gray-zone.

This study demonstrates the feasibility of employing ML models as substitutes for conventional CP scheme within the high-resolution weather forecasting model. Future efforts will focus on the development of ML models, based on data generated by super-parameterization or cloud-resolving models, to replace conventional CP schemes in weather forecasting models. The objective of this substitution is to reduce uncertainties and improve performance of weather forecast models.

385 *Code and data availability.* The source code for the WRF model version 4.3 used in this study is available at <https://doi.org/10.5281/zenodo.10039053> (Skamarock et al., 2023). The source code and data used in this are available at <https://doi.org/10.5281/zenodo.10032404> (Zhong et al., 2023b).

Author contributions. X.Z. trained the deep learning models and calculate the statistics of model performance. X.Y. and X.Z. conducted the WRF simulations to provide dataset for training and evaluation, and offered valuable suggestions on the model training and paper revision.

390 X.Z. and X.Y. wrote, reviewed and edited the original draft; X.Z., X.Y., and H.L. supervised and supported this research and gave important opinions. All of the authors have contributed to and agreed to the published version of the manuscript.

Competing interests. The authors declare no conflict of interest.

Acknowledgements. This work was supported by Basic and Applied Basic Research Foundation of Guangdong Province, under Grant No. 2021A1515012582. We are thankful for Mesoscale and Microscale Meteorology Laboratory (MMM) at NCAR for developing and sharing

395 the WRF source codes.

References

- Arakawa, A.: The Cumulus Parameterization Problem: Past, Present, and Future, *Journal of Climate*, 17, 2493 – 2525, [https://doi.org/https://doi.org/10.1175/1520-0442\(2004\)017<2493:RATCPP>2.0.CO;2](https://doi.org/https://doi.org/10.1175/1520-0442(2004)017<2493:RATCPP>2.0.CO;2), 2004.
- Bougeault, P. and Lacarrère, P.: Parameterization of orographic induced turbulence in a mesobeta scale model, *Monthly Weather Review*, 117, 1872–1890, [https://doi.org/10.1175/1520-0493\(1989\)117<1872:POOITI>2.0.CO;2](https://doi.org/10.1175/1520-0493(1989)117<1872:POOITI>2.0.CO;2), 1989.
- 400 Brenowitz, N. D. and Bretherton, C. S.: Prognostic Validation of a Neural Network Unified Physics Parameterization, *Geophysical Research Letters*, 45, 6289–6298, <https://doi.org/https://doi.org/10.1029/2018GL078510>, 2018.
- Brenowitz, N. D. and Bretherton, C. S.: Spatially Extended Tests of a Neural Network Parametrization Trained by Coarse-Graining, *Journal of Advances in Modeling Earth Systems*, 11, 2728–2744, <https://doi.org/https://doi.org/10.1029/2019MS001711>, 2019.
- 405 Chan, S. C., Kendon, E. J., Fowler, H. J., Blenkinsop, S., Ferro, C. A. T., and Stephenson, D. B.: Does increasing the spatial resolution of a regional climate model improve the simulated daily precipitation?, *Climate Dynamics*, 41, 1475–1495, <https://doi.org/10.1007/s00382-012-1568-9>, 2013.
- Clark, A. J. et al.: An Overview of the 2010 Hazardous Weather Testbed Experimental Forecast Program Spring Experiment, *Bulletin of the American Meteorological Society*, 93, 55 – 74, <https://doi.org/10.1175/BAMS-D-11-00040.1>, 2012.
- 410 Di, X. R., Xiong, Z. S., and Beijing: A Study of Circumstances of Meso- β -Scale Systems of Strong Heavy Rainfall in Warm Sector Ahead of Fronts in South China, *Chinese Journal of Atmospheric Sciences/Daqii kexue*, 2006.
- Ding, Y.: *Seasonal march of the East-Asian summer monsoon*, World Scientific, 2004.
- Gentine, P., Pritchard, M., Rasp, S., Reinaudi, G., and Yacalis, G.: Could Machine Learning Break the Convection Parameterization Dead-lock?, *Geophysical Research Letters*, 45, 5742–5751, <https://doi.org/https://doi.org/10.1029/2018GL078202>, 2018.
- 415 Giorgi, F., Torma, C., Coppola, E., Ban, N., Schär, C., and Somot, S.: Enhanced summer convective rainfall at Alpine high elevations in response to climate warming, *Nature Geoscience*, 9, 584–589, <https://doi.org/10.1038/ngeo2761>, 2016.
- Grell, G. A. and Dévényi, D.: A generalized approach to parameterizing convection combining ensemble and data assimilation techniques, *Geophysical Research Letters*, 29, 38–1, 2002.
- Grell, G. A. and Freitas, S. R.: A scale and aerosol aware stochastic convective parameterization for weather and air quality modeling, *Atmospheric Chemistry and Physics*, 14, 5233–5250, <https://doi.org/10.5194/acp-14-5233-2014>, 2014.
- 420 Han, J. and Pan, H.-L.: Revision of convection and vertical diffusion schemes in the NCEP Global Forecast System, *Weather and Forecasting*, 26, 520–533, 2011.
- Han, Y., Zhang, G. J., Huang, X., and Wang, Y.: A Moist Physics Parameterization Based on Deep Learning, *Journal of Advances in Modeling Earth Systems*, 12, e2020MS002076, <https://doi.org/https://doi.org/10.1029/2020MS002076>, e2020MS002076 2020MS002076, 2020.
- 425 He, K., Zhang, X., Ren, S., and Sun, J.: Deep residual learning for image recognition, in: *Proceedings of the IEEE conference on computer vision and pattern recognition*, pp. 770–778, 2016.
- Hersbach, H., Bell, B., Berrisford, P., Hirahara, S., Horányi, A., Muñoz-Sabater, J., Nicolas, J., Peubey, C., Radu, R., Schepers, D., et al.: The ERA5 global reanalysis, *Quarterly Journal of the Royal Meteorological Society*, 146, 1999–2049, 2020.
- Hong, S.-Y. and Dudhia, J.: Next-Generation Numerical Weather Prediction: Bridging Parameterization, Explicit Clouds, and Large Eddies, *Bulletin of the American Meteorological Society*, 93, ES6 – ES9, <https://doi.org/https://doi.org/10.1175/2011BAMS3224.1>, 2012.
- 430 Hong, S.-Y. and Lim, J.-O. J.: The WRF single-moment 6-class microphysics scheme (WSM6), *Asia-Pacific Journal of Atmospheric Sciences*, 42, 129–151, 2006.

- Iacono, M. J., Delamere, J. S., Mlawer, E. J., Shephard, M. W., Clough, S. A., and Collins, W. D.: Radiative forcing by long-lived greenhouse gases: Calculations with the AER radiative transfer models, *Journal of Geophysical Research: Atmospheres*, 113, 2008.
- 435 Janjic, Z.: The surface layer parameterization in the NCEP Eta Model, World Meteorological Organization-Publications-WMO TD, pp. 4–16, 1996.
- Jeworrek, J., West, G., and Stull, R.: Evaluation of Cumulus and Microphysics Parameterizations in WRF across the Convective Gray Zone, *Weather and Forecasting*, 34, 1097 – 1115, <https://doi.org/https://doi.org/10.1175/WAF-D-18-0178.1>, 2019.
- Jian, S., Ping, Z., and Xiuji, Z.: THE MESOSCALE STRUCTURE OF A SOUTH CHINA RAINSTORM AND THE INFLUENCE OF
440 COMPLEX TOPOGRAPHY (in Chinese), *Acta Meteorologica Sinica*, pp. 333–342, <https://doi.org/10.11676/qxxb2002.040>, 2002.
- Johnson, A., Wang, X., Kong, F., and Xue, M.: Object-Based Evaluation of the Impact of Horizontal Grid Spacing on Convection-Allowing Forecasts, *Monthly Weather Review*, 141, 3413 – 3425, <https://doi.org/https://doi.org/10.1175/MWR-D-13-00027.1>, 2013.
- Kain, J. S.: The Kain–Fritsch Convective Parameterization: An Update, *Journal of Applied Meteorology*, 43, 170 – 181, [https://doi.org/https://doi.org/10.1175/1520-0450\(2004\)043<0170:TKCPAU>2.0.CO;2](https://doi.org/https://doi.org/10.1175/1520-0450(2004)043<0170:TKCPAU>2.0.CO;2), 2004.
- 445 Kain, J. S. and Fritsch, J. M.: A One-Dimensional Entraining/Detraining Plume Model and Its Application in Convective Parameterization, *Journal of Atmospheric Sciences*, 47, 2784 – 2802, [https://doi.org/https://doi.org/10.1175/1520-0469\(1990\)047<2784:AODEPM>2.0.CO;2](https://doi.org/https://doi.org/10.1175/1520-0469(1990)047<2784:AODEPM>2.0.CO;2), 1990.
- Kain, J. S. and Fritsch, J. M.: Convective Parameterization for Mesoscale Models: The Kain-Fritsch Scheme, pp. 165–170, American Meteorological Society, Boston, MA, https://doi.org/10.1007/978-1-935704-13-3_16, 1993.
- 450 Kingma, D. P. and Ba, J.: Adam: A Method for Stochastic Optimization, 2014.
- Krasnopolsky, V. M., Fox-Rabinovitz, M. S., and Belochitski, A. A.: Using ensemble of neural networks to learn stochastic convection parameterizations for climate and numerical weather prediction models from data simulated by a cloud resolving model, *Advances in Artificial Neural Systems*, 2013, 5–5, 2013.
- Lean, H. W., Clark, P. A., Dixon, M., Roberts, N. M., Fitch, A., Forbes, R., and Halliwell, C.: Characteristics of High-Resolution Versions
455 of the Met Office Unified Model for Forecasting Convection over the United Kingdom, *Monthly Weather Review*, 136, 3408 – 3424, <https://doi.org/10.1175/2008MWR2332.1>, 2008.
- Li, Z., Kovachki, N., Azizzadenesheli, K., Liu, B., Bhattacharya, K., Stuart, A., and Anandkumar, A.: Fourier neural operator for parametric partial differential equations, arXiv preprint arXiv:2010.08895, 2020.
- Livneh, B., Restrepo, P. J., and Lettenmaier, D. P.: Development of a unified land model for prediction of surface hydrology and land–
460 atmosphere interactions, *Journal of Hydrometeorology*, 12, 1299–1320, 2011.
- Luo, Y., Zhang, R., Wan, Q., Wang, B., Wong, W. K., Hu, Z., Jou, B. J.-D., Lin, Y., Johnson, R. H., Chang, C.-P., Zhu, Y., Zhang, X., Wang, H., Xia, R., Ma, J., Zhang, D.-L., Gao, M., Zhang, Y., Liu, X., Chen, Y., Huang, H., Bao, X., Ruan, Z., Cui, Z., Meng, Z., Sun, J., Wu, M., Wang, H., Peng, X., Qian, W., Zhao, K., and Xiao, Y.: The Southern China Monsoon Rainfall Experiment (SCMREX), *Bulletin of the American Meteorological Society*, 98, 999 – 1013, <https://doi.org/https://doi.org/10.1175/BAMS-D-15-00235.1>, 2017.
- 465 Mishra, S. K., Anand, A., Fasullo, J., and Bhagat, S.: Importance of the Resolution of Surface Topography in Indian Monsoon Simulation, *Journal of Climate*, 31, 4879 – 4898, <https://doi.org/https://doi.org/10.1175/JCLI-D-17-0324.1>, 2018.
- O’Gorman, P. A. and Dwyer, J. G.: Using Machine Learning to Parameterize Moist Convection: Potential for Modeling of Climate, Climate Change, and Extreme Events, *Journal of Advances in Modeling Earth Systems*, 10, 2548–2563, <https://doi.org/https://doi.org/10.1029/2018MS001351>, 2018.

- 470 Onishi, R., Hirai, J., Kolomenskiy, D., and Yasuda, Y.: Real-Time High-Resolution Prediction of Orographic Rainfall for Early Warning of Landslides, pp. 237–248, Springer International Publishing, Cham, https://doi.org/10.1007/978-3-031-16898-7_17, 2023.
- Ou, T., Chen, D., Chen, X., Lin, C., Yang, K., Lai, H.-W., and Zhang, F.: Simulation of summer precipitation diurnal cycles over the Tibetan Plateau at the gray-zone grid spacing for cumulus parameterization, *Climate Dynamics*, 54, 3525–3539, 2020.
- Rasp, S.: Coupled online learning as a way to tackle instabilities and biases in neural network parameterizations: general algorithms and Lorenz 96 case study (v1.0), *Geoscientific Model Development*, 13, 2185–2196, <https://doi.org/10.5194/gmd-13-2185-2020>, 2020.
- 475 Rasp, S., Pritchard, M. S., and Gentine, P.: Deep learning to represent subgrid processes in climate models, *Proceedings of the National Academy of Sciences*, 115, 9684–9689, <https://doi.org/10.1073/PNAS.1810286115>, 2018.
- Ren, S., He, K., Girshick, R., and Sun, J.: Faster R-CNN: Towards Real-Time Object Detection with Region Proposal Networks, 2016.
- Roberts, N. M. and Lean, H. W.: Scale-selective verification of rainfall accumulations from high-resolution forecasts of convective events, 480 *Monthly Weather Review*, 136, 78–97, 2008.
- Schumacher, V., Fernández, A., Justino, F., and Comin, A.: WRF high resolution dynamical downscaling of precipitation for the Central Andes of Chile and Argentina, *Frontiers in Earth Science*, 8, 328, 2020.
- Schwartz, C. S.: Reproducing the September 2013 Record-Breaking Rainfall over the Colorado Front Range with High-Resolution WRF Forecasts, *Weather and Forecasting*, 29, 393 – 402, <https://doi.org/https://doi.org/10.1175/WAF-D-13-00136.1>, 2014.
- 485 Skamarock, W. C., Klemp, J. B., Dudhia, J., Gill, D. O., Liu, Z., Berner, J., Wang, W., Powers, J., Duda, M., Barker, D., et al.: A description of the advanced research WRF version 4, NCAR tech. note ncar/tn-556+ str, 145, <https://doi.org/doi:10.5065/1dfh-6p97>, 2019.
- Skamarock, W. C., Klemp, J. B., Dudhia, J., Gill, D. O., Liu, Z., Berner, J., Wang, W., Powers, J. G., Duda, M. G., Barker, D. M., and Xiang-yu, H.: A Description of the Advanced Research WRF Model Version 4.3, National Center for Atmospheric Research: Boulder, CO, USA, <https://doi.org/doi:10.5065/1dfh-6p97>, 2021.
- 490 Skamarock, W. C., Klemp, J. B., Dudhia, J., Gill, D. O., Liu, Z., Berner, J., Wang, W., Powers, J., Duda, M., Barker, D., et al.: The source codes of WRF-V4.3 and WPS-V4.3 [Software]. Zenodo. <https://doi.org/10.5281/zenodo.10039053>, 2023.
- Tao, S. Y.: Storm Rainfall in China (in Chinese)., Science Press, Beijing, 1981.
- Vaswani, A., Shazeer, N., Parmar, N., Uszkoreit, J., Jones, L., Gomez, A. N., Kaiser, Ł., and Polosukhin, I.: Attention is all you need, *Advances in neural information processing systems*, 30, 2017.
- 495 Villalba-Pradas, A. and Tapiador, F. J.: Empirical values and assumptions in the convection schemes of numerical models, *Geoscientific Model Development*, 15, 3447–3518, <https://doi.org/10.5194/gmd-15-3447-2022>, 2022.
- Wyngaard, J. C.: Toward Numerical Modeling in the “Terra Incognita”, *Journal of the Atmospheric Sciences*, 61, 1816 – 1826, [https://doi.org/https://doi.org/10.1175/1520-0469\(2004\)061<1816:TNMITT>2.0.CO;2](https://doi.org/https://doi.org/10.1175/1520-0469(2004)061<1816:TNMITT>2.0.CO;2), 2004.
- Xia, R. and Zhao, S.: Diagnosis and modeling of meso–scale systems of heavy rainfall in warm sector ahead of front in South China (middle 500 part of Guangdong province) in June 2005, *Chinese journal of atmospheric sciences/Daqi Kexue*, 33, 2009.
- Yao, Y., Zhong, X., Zheng, Y., and Wang, Z.: A Physics-Incorporated Deep Learning Framework for Parameterization of Atmospheric Radiative Transfer, *Journal of Advances in Modeling Earth Systems*, 15, e2022MS003445, <https://doi.org/https://doi.org/10.1029/2022MS003445>, e2022MS003445 2022MS003445, 2023.
- Yuval, J. and O’Gorman, P. A.: Stable machine-learning parameterization of subgrid processes for climate modeling at a range of resolutions, 505 *Nature communications*, 11, 3295, 2020.
- Yuval, J., O’Gorman, P. A., and Hill, C. N.: Use of neural networks for stable, accurate and physically consistent parameterization of subgrid atmospheric processes with good performance at reduced precision, *Geophysical Research Letters*, 48, e2020GL091363, 2021.

- Zhang, X. and Ni, Y.: A comparative study of a frontal and a non-frontal convective systems, *Acta Meteorologica Sinica*, pp. 108–121, <https://doi.org/10.11676/qxxb2009.012>, 2009.
- 510 Zhang, X., Bao, J.-W., Chen, B., and Huang, W.: Evaluation and Comparison of Two Deep Convection Parameterization Schemes at Convection-Permitting Resolution, *Monthly Weather Review*, 149, 3419 – 3432, <https://doi.org/https://doi.org/10.1175/MWR-D-21-0016.1>, 2021.
- Zhao, P., Zhang, R., Liu, J., Zhou, X., and He, J.: Onset of southwesterly wind over eastern China and associated atmospheric circulation and rainfall, *Climate Dynamics*, 28, 797–811, 2007.
- 515 Zheng, Y., Alapaty, K., Herwehe, J. A., Genio, A. D. D., and Niyogi, D.: Improving High-Resolution Weather Forecasts Using the Weather Research and Forecasting (WRF) Model with an Updated Kain–Fritsch Scheme, *Monthly Weather Review*, 144, 833 – 860, <https://doi.org/https://doi.org/10.1175/MWR-D-15-0005.1>, 2016.
- Zhong, L., Mu, R., Zhang, D., Zhao, P., Zhang, Z., and Wang, N.: An observational analysis of warm-sector rainfall characteristics associated with the 21 July 2012 Beijing extreme rainfall event, *Journal of Geophysical Research*, 120, 3274–3291, 2015.
- 520 Zhong, S. and Chen, Z.: The Impacts of Atmospheric Moisture Transportation on Warm Sector Torrential Rains over South China, *Atmosphere*, 8, <https://doi.org/10.3390/atmos8070116>, 2017.
- Zhong, X., Ma, Z., Yao, Y., Xu, L., Wu, Y., and Wang, Z.: WRF–ML v1.0: a bridge between WRF v4.3 and machine learning parameterizations and its application to atmospheric radiative transfer, *Geoscientific Model Development*, 16, 199–209, <https://doi.org/10.5194/gmd-16-199-2023>, 2023a.
- 525 Zhong, X., Yu, X., and Li, H.: Machine Learning Parameterization of the Multi-scale Kain-Fritsch (MSKF) Convection Scheme and stable simulation coupled in WRF using WRF-ML v1.0 (Version 1.0) [Dataset] [Software]. Zenodo. <https://doi.org/10.5281/zenodo.10032404>, 2023b.